UC Berkeley
Research Reports

Title
Vehicle Lane Change Maneuver In Automated Highway Systems

Permalink
https://escholarship.org/uc/item/29j5s3gk

Authors
Chee, Wonshik
Tomizuka, Masayoshi

Publication Date
1994

Vehicle Lane Change Maneuver in Automated Highway Systems

Wonshik Chee
Masayoshi Tomizuka

The contents of this report reflect the views of the authors who are responsible
for the facts and the accuracy of the data presented herein. The contents do not
necessarily reflect the official views or policies of the State of California. This
report does not constitute a standard, specification, or regulation.

CALIFORNIA PARTNERS FOR ADVANCED TRANSIT AND HIGHWAYS

Vehicle Lane Change Maneuver in Automated Highway Systems

Wonshik Chee
Masayoshi Tomizuka

Final Copy
MOU 89

October 1994

Vehicle Lane Change Maneuver in Automated Highway Systems

Vehicle Lane Change Maneuver in Automated Highway Systems

Wonshik Chee, Graduate Student Researcher
Masayoshi Tomizuka, Professor

Department of Mechanical Engineering
University of California, Berkeley, CA 94720

Abstract

This report is concerned with lane change maneuver in automated highway systems. In this problem, a vehicle, initially under closed loop lane following control on an automated lane, must be guided to the adjacent automated lane. The desired trajectory between two automated lanes is designed by considering the transition time from one lane to another lane and passenger's ride comfort. Four types of the desired trajectories are considered. The nominal steering input that can make the vehicle follow the desired trajectory in the absence of model uncertainties and disturbances is obtained by inverting a linear dynamic model, which relates the steering input to the vehicle lateral displacement. Simulations show that the nominal input alone cannot assure an acceptable level of maneuvering accuracy in the presence of uncertainties and disturbances such as wind gusts and changes in the tire cornering stiffness. The use of onboard sensors for the closed loop control can significantly improve performance. Three closed loop controllers, based on (i) linear quadratic (LQ) optimal control, (ii) frequency shaped linear quadratic (FSLQ), and (iii) sliding mode control will be evaluated for this application. Simulation results show that these controllers provide acceptable performance in the presence of uncertainties and disturbances.

Executive Summary

In this report, lane change maneuver for an automated highway system is investigated as a tracking problem with respect to the virtual desired trajectory (VDT). The two main issues discussed in the report are: 1) design of virtual desired trajectory and 2) design of control algorithms.

The VDT is a desired trajectory for lane change maneuver. The word "virtual" implies that controllers for lane change maneuver do not have physical access to the desired trajectory. Therefore, lane change maneuver is performed in an open loop manner with aid from onboard sensors to reduce sensitivity to the uncertainties. The VDT's are designed to give good ride quality by placing constraints on lateral acceleration and jerk. Another important consideration while designing VDT's is minimization of the transition time. Four types of the VDT are studied in this report: 1) the circular trajectory, 2) the cosine approximation to the circular trajectory, 3) the polynomial trajectory, and 4) the trapezoidal acceleration trajectory. Considering simplicity of specifying the ride comfort quality parameters to the VDTs and the required maneuver time, we select the trapezoidal acceleration trajectory as the VDT for lane change maneuvers.

Three control algorithms are designed: 1) the linear quadratic (LQ) optimal control algorithm, 2) the frequency shaped linear quadratic (FSLQ) optimal control algorithm, and 3) the sliding mode control algorithm using a filtered error. Frequency shaping is incorporated in to the cost function by having frequency dependent weights on the position error, the yaw rate, and the lateral acceleration. The objective of the frequency shaping is to improve ride comfort in the frequency range where human passengers are sensitive and to reduce sensitivity to the system uncertainties at high frequencies. For the sliding mode controller, the error signal is processed by a first order low pass filter. Then, the sliding surface is designed using this filtered error signal. The effect of the filter on the controller is a smoother control command, as compared to the sliding mode controller using an integrated error signal. Therefore, the system response is smoother with corresponding improvement in ride comfort.

From the simulation results under various operating conditions, it can be concluded that both the FSLQ optimal controller and the sliding mode controller using filtered error will achieve good tracking performance.

1. Introduction

Automated highway systems (AHS), or more broadly intelligent vehicle and highway systems (IVHS) technologies, attempt computerized control of vehicles on highways to enhance the safety and improve the efficiency of highways. A crucial part of AHS is the lateral control of vehicles, which includes lane following and lane change maneuvers. A substantial amount of research has been conducted on the lane following problem. Peng and Tomizuka (1990) formulated several models of the vehicle and applied the frequency shaped linear quadratic (FSLQ) optimal approach to design a lane following controller. This controller provides a compromise between the two major design considerations: lane tracking performance and passenger's comfort. Furthermore, they developed an optimal preview controller for lane following maneuvers (Peng and Tomizuka 1991). The FSLQ and optimal preview control algorithm have been experimentally tested, and their effectiveness has been demonstrated (Hessburg et al 1991, Peng 1992). A fuzzy rule-based controller for lane following has also been designed (Hessburg and Tomizuka 1994).

In contrast to lane following maneuvers, considerably less research has been conducted for the lane change maneuvers. There were some efforts to design a controller based on a model of a human driver, which is relevant to both the lane change and the lane following maneuver problem. Godthelp (1983) investigated human driving patterns, and found that, during a lane change, the steering wheel angle of a vehicle resembles a sine function. He also found that the lane change maneuver may be divided into four phases according to the signs of steering angle and its time derivative. Hess and Modjtahezadeh (1989) proposed a preview controller model of a human driver for a lane following and a lane change maneuver.

The objective of a lane change maneuver in AHS is to develop an optimal method to transfer a vehicle, which is under closed loop lane following control on an automated lane, to the adjacent lane. This report describes 1) the determination of the optimal trajectory for the vehicles to follow between two automated lanes, and 2) the comparison of several closed-loop control schemes for a lane change maneuver using on-board sensors as feedback measurements.

The optimal trajectory is designed by considering passenger's comfort and the required transition time for the maneuver. The trajectory may be physically marked on highways if lane changes are allowed at specified lane transition sections. However, in this report, it is assumed that lane changes may take place anywhere and the desired

trajectory is not marked on highways. The desired trajectory is coded by software in the onboard computer aboard a vehicle. Because of this assumption, the desired trajectory is called the virtual desired trajectory (VDT). Kanayama and Hartman (1989) proposed continuous curvature trajectories for various situations including a lane change maneuver in which the trajectory connects two parallel lines. Although the resulting trajectory has continuous curvature, which is necessary to make the control input smooth, their design method involves an implicit function of time that needs large number of computation. Nelson (1989) proposed two types of curves: (i) polar polynomials in place of circular-arc segments, and (ii) Cartesian polynomials in place of arc-line-arc segments for lane change maneuvers. These curves are computationally simple and have closed-form expressions that provide continuous curvature. However, they have drawbacks in that they are not expressed in terms of time and it is difficult to incorporate the ride comfort constraints in them.

In this report, four trajectories for the lane change maneuver are designed using the transition time as a performance index, the maximum allowable lateral acceleration and jerk as constraints, and longitudinal speed as a design parameter. The criteria for selecting the optimal trajectory are the time required to complete a lane change maneuver and the maximum lateral acceleration produced.

The acceleration and jerk will remain within comfortable levels for passengers by controlling the vehicle to follow the VDT. Since there exists a significant amount of uncertainty in the vehicle dynamics, the controller must be robust. To achieve this goal, a linear quadratic (LQ) optimal controller, a frequency shaped linear quadratic (FSLQ) optimal controller and a sliding mode controller using a filtered error signal will be designed and their performances will be compared through simulations in this report.

This report is organized as follows. Section 2 gives the description of the vehicle dynamics, followed by design of the VDT's in section 3. Uncertainty analysis is presented in section 4. Section 5 and 6 describe the LQ/FSLQ and the sliding mode controller respectively. Section 7 summarizes the simulation results, and section 8 will present conclusions.

2. System Description

Both nonlinear and linear models for the lateral motion of a vehicle were developed by Peng and Tomizuka (1990,1992). The simplified model (Peng and Tomizuka 1990) can be written as

$$\ddot{y} = \frac{A_1}{V}\dot{y} - A_1\varepsilon + \frac{A_2}{V}\dot{\varepsilon} + B_1\delta - \frac{K_y}{m}\{V_{wy} - V\varepsilon + \dot{y}\}|V_{wy} - V\varepsilon + \dot{y}| \tag{1}$$

$$\ddot{\varepsilon} = \frac{A_3}{V}\dot{y} - A_3\varepsilon + \frac{A_4}{V}\dot{\varepsilon} + B_2\delta \tag{2}$$

where y and ε are the lateral position, and the yaw angle of the vehicle (measured from an inertial reference), respectively. The front wheel steering angle is denoted by δ. The vehicle longitudinal velocity is denoted by V and assumed to be constant during lane change maneuvers. V_{wy} is the velocity of the lateral wind. All other parameters are treated as constants. The nonlinear term in equation (1), which represents the wind drag due to lateral wind, is included in order to consider the lateral wind force. A_i's and B_i's in equation (1) and (2) are defined by

$$A_1 = \frac{-4.0C_s}{m}, A_2 = \frac{-2.0C_s(l_1 - l_2)}{m}, A_3 = \frac{-2.0C_s(l_1 - l_2)}{I_z}, A_4 = \frac{-2.0C_s(l_1^2 - l_2^2)}{I_z}$$

$$B_1 = \frac{2.0C_s}{m} \text{ ,and } B_2 = \frac{2.0C_s l_1}{I_z} \tag{3}$$

Vehicle parameters, C_s, l_1, l_2, m, and I_z, along with their nominal values are defined in Table 1.
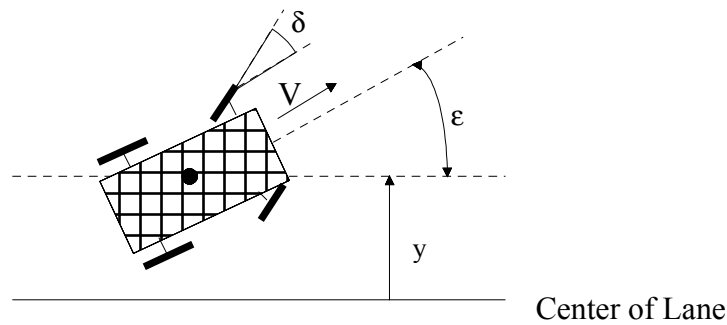

Figure 1: Simplified Model of a Vehicle

Symbol	Description	Nominal Value
V	Speed of Vehicle	31.1 (m/sec)
C_s	Cornering Stiffness	57200 (N/rad)
m	Mass	1465 (kg)
I_z	Moment of Inertia About Vertical Axis	2900 (kg-m^2)
K_y	Lateral Drag Coefficient	0.45
l_1	Distance from Center of Gravity to Front Axle	1.12 (m)
l_2	Distance from Center of Gravity to Rear Axle	1.41 (m)

Table 1: Definition of Vehicle Parameters

Sensors for this system include a lateral accelerometer and a yaw rate sensor. The magnetometer used in the lane following control to measure the distance between the position of a vehicle and the center line of a lane is not used here because it is assumed that there is no marker between the lanes. Thus, the position of the vehicle is obtained by integrating the signal from the lateral accelerometer twice. Yaw angle of the vehicle is obtained from the yaw rate sensor by one integration.

Actuator dynamics is not considered in the selection of the desired trajectory and the controller design. However, in simulation, the actuator dynamics is included. The actuator dynamics is assumed to be first order, i.e.

$$\frac{d\delta_a}{dt} = \frac{1}{\tau_{steer}}(\delta_c - \delta_a) \tag{4}$$

where δ_a and δ_c are the actual and the command steering angle, respectively, and τ_{steer} is the time constant of the actuator. In the simulations, the complex model (Peng 1992), which includes all six degree of freedom of the vehicle motion as well as a nonlinear tire model, is used to verify the controller.

3. Virtual Desired Trajectory (VDT)

As mentioned before, the desired trajectory for a lane change maneuver is designed by considering passenger's ride comfort and transition time. Caywood and et. al. (1977) proposed that, for ride comfort, the transient lateral acceleration and the associated jerk should not exceed 0.12 g and 0.24 g/s, respectively. For the design of the virtual desired trajectory (VDT), the lateral acceleration limit and the lateral jerk limit are taken as 0.05 g and 0.1 g/s, respectively. These values are chosen to allow ride quality margin for controller action.

Four candidates for the VDT have been designed using the transition time as a performance index, the maximum allowable lateral acceleration as a constraint, and speed of the vehicle as a design parameter. Speed of the vehicle is assumed to be constant during the lane change maneuver and is taken as 31.1 m/sec (70 MPH). The VDTs are

(1) Circular trajectory
(2) Cosine trajectory
(3) 5th order polynomial trajectory
(4) Trapezoidal acceleration trajectory.

The first two do not satisfy the specified jerk constraints for proper ride comfort, and are introduced for setting standards for the last two trajectories.

(1) Circular trajectory

This trajectory consists of two circular arcs with a curvature equal in magnitude but opposite in direction, and a straight segment between the two arcs as shown in figure 2. The radius of curvature, ρ, for the circular sections is

$$\rho = \frac{V^2}{a_{max}} \tag{5}$$

where V is the longitudinal speed and a_{max} is the maximum allowable lateral acceleration. In figure 2, y is the lateral displacement of the vehicle relative to the initial lane, d is the width of a lane, t_c is the time that corresponds to the circular portion of the trajectory, and

t_s is the time that corresponds to the straight line portion of the trajectory. The radius of curved section is defined by ρ, which is determined by equation (5).
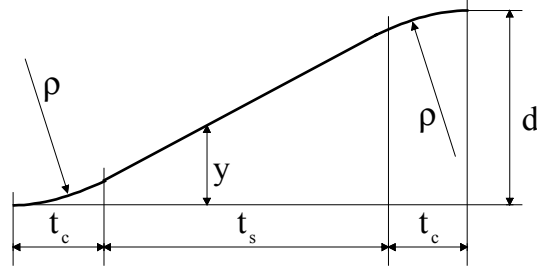

Figure 2: Definition of the Variables for Circular Trajectory

These parameters must satisfy the geometric constraint as follows.

$$d = 2\rho\left(1 - \cos\frac{V}{\rho}t_c\right) + Vt_s\sin\frac{V}{\rho}t_c \tag{6}$$

The transition time (T_{cir}) is

$$T_{cir} = t_s + 2t_c. \tag{7}$$

Solving equation (6) for t_s, equation (7) becomes

$$T_{cir} = 2t_c + \frac{(d - 2\rho)}{V\sin\left(\frac{V}{\rho}t_c\right)} + 2\frac{\rho}{V}\cot\left(\frac{V}{\rho}t_c\right). \tag{8}$$

Notice that T_{cir} is a function of t_c. To find the minimum transition time, equation (8) is differentiated with respect to t_c to obtain

$$\frac{dT_{cir}}{dt_c} = 2 - \left(\frac{d}{\rho} - 2\right)\frac{\cos\left(\frac{Vt_c}{\rho}\right)}{\sin^2\left(\frac{Vt_c}{\rho}\right)} - 2\frac{1}{\sin^2\left(\frac{Vt_c}{\rho}\right)}. \tag{9}$$

From this, $\dfrac{dT_{cir}}{dt_c}$ is zero for

$$t_c = \frac{\rho}{V}\cos^{-1}\left(1-\frac{d}{2\rho}\right). \tag{10}$$

For this t_c, we can confirm from equation (6) that t_s is zero. This means that the trajectory should not have any straight section in order to achieve the minimum transition time. Therefore, the optimal trajectory is written as

$$y(t) = \rho\left(1-\cos\frac{V}{\rho}t\right) \quad , \quad 0 \le t \le t_c$$

$$\tag{11}$$

$$\rho\left\{1+\cos\frac{V}{\rho}(T-t)-2\cos\frac{V}{\rho}t_c\right\} \quad , \quad t_c \le t \le T$$

and the required transition time is

$$T_{cir} = \frac{2\rho}{V}\cos^{-1}\left(1-\frac{d}{2\rho}\right) \cong \frac{2\rho}{V}\sqrt{\frac{d}{\rho}} = 2\sqrt{\frac{d}{a_{\max}}}. \tag{12}$$

This trajectory is shown in figure 3 for $V = 31.3$ m/s (70 MPH) and $a_{\max} = 0.05$g. Although this trajectory satisfies the acceleration constraint for ride comfort, the jerk constraint has been ignored. In fact, the jerk is infinity at $t = 0$, t_c, and $2\,t_c$.

(2) Cosine Approximation

Equation (11) motivates a trajectory of the form,

$$y(t) = \frac{d}{2}\left\{1-\cos\left(\frac{t}{T}\pi\right)\right\} \quad , \quad 0 \le t \le T \tag{13}$$

where T is taken as the same value as T_{cir}. The second derivative of this $y(t)$ is

$$\ddot{y}(t) = \frac{d}{2}\left(\frac{\pi}{T_{cir}}\right)^2\cos\left(\frac{\pi t}{T_{cir}}\right). \tag{14}$$
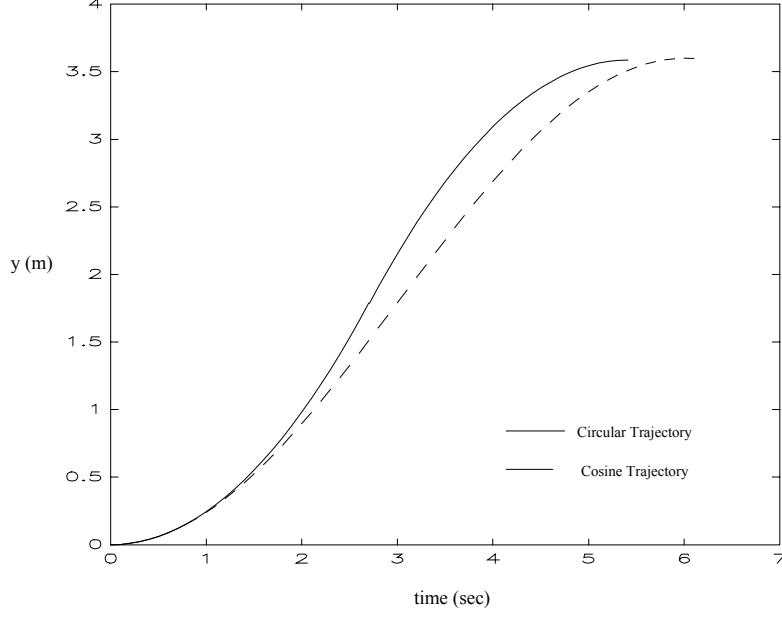
Figure 3: Virtual Desired Trajectories

The maximum lateral acceleration generated from this trajectory exceeds the lateral acceleration constraint. Therefore, equation (13) is modified as

$$y(t) = \frac{d}{2}\{1 - \cos(\alpha t)\} \quad , \quad 0 \le \alpha t \le \pi \tag{15}$$

to satisfy the acceleration limit. Then, the second derivative for this trajectory becomes

$$\ddot{y}(t) = \frac{d\alpha^2}{2}\cos(\alpha t). \tag{16}$$

Although $\ddot{y}$ is normal to the lane and is not exactly in the direction normal to the vehicle, it is still a good indicator for the lateral acceleration for $\frac{V\pi}{\alpha} \gg d$, which is normally the case.

To satisfy the acceleration constraint, α is selected as

$$\alpha = \sqrt{\frac{2 a_{max}}{d}}. \tag{17}$$

Then, the transition time becomes

$$T_{cos} = \pi \sqrt{\frac{d}{2a_{max}}}. \tag{18}$$

Note that $T_{cos} > T_{cir}$ and that $\ddot{y}$ is still discontinuous at $t = 0$ and $t = T_{cos}$. Comparing the circular trajectory and the cosine trajectory, the latter removes the discontinuity of the second derivative at the midpoint of the trajectory at the expense of the increased transition time. This trajectory is shown in figure 3.

The trajectories introduced above have discontinuous second derivatives. While it may be argued that the first order steering actuator dynamics, equation (4), will cause the lateral jerk to remain finite at the discontinuities of the lateral acceleration, this is not a satisfactory argument from the view point of tracking controller design. Two trajectories, which satisfy the jerk constraint, are given below.

(3) Polynomial Trajectory

Nelson (1989) proposed two types of curves: polar polynomials in place of circular-arc segments, and Cartesian polynomials in place of arc-line-arc segments for lane change maneuvers. These curves are computationally simple and have closed-form expressions that provide continuous curvature. Although these polynomials are in closed forms, it is still difficult to use them because they are not parameterized with respect to transition time and proper ride comfort constraints. For lane change maneuvers, Nelson proposed a 5th order polynomial to describe the lateral position as a function of the longitudinal position of the vehicle. However, in view of the fact that the longitudinal position might not be easily available, the trajectory is modified to be a function of time in this report. The main advantage of the polynomial trajectory is that the resulting curvature is 3 times differentiable along the trajectory.

The trajectory is expressed by

$$y(x) = d\left\{ 10\left(\frac{x}{x_e}\right)^3 - 15\left(\frac{x}{x_e}\right)^4 + 6\left(\frac{x}{x_e}\right)^5 \right\} \tag{19}$$

where x is the longitudinal position of the vehicle relative to the starting point of the trajectory and x_e is the terminal point of the trajectory, which is determined from the lateral acceleration limit.

If we assume $d \ll x_e$, then $\dfrac{d}{x_e} \ll 1$. Thus, we can assume $\dfrac{dy}{dx} \ll 1$, and the curvature, κ, can be approximated as

$$\kappa = \frac{\dfrac{d^2 y}{dx^2}}{\sqrt{1 + \left(\dfrac{dy}{dx}\right)^2}} \approx \frac{d^2 y}{dx^2}. \tag{20}$$

With this assumption, the following relation can be established

$$V\, dt = dx \sqrt{1 + \left(\frac{dy}{dx}\right)^2} \approx dx, \text{ or } \frac{dt}{dx} = \frac{1}{V}. \tag{21}$$

Thus, κ can be related to the lateral acceleration by

$$\kappa = \frac{d^2 y}{dx^2} = \frac{1}{V^2} \cdot \left. \frac{d^2 y}{dt^2} \right|_{t=\frac{x}{V}}. \tag{22}$$

Letting x_m denote the position where the curvature is maximum, $\dfrac{x_m}{x_e}$ can be determined by solving $\dfrac{d\kappa}{dx} = 0$.

$$\left. \frac{d\kappa}{dx} \right|_{x=x_m} = \left. \frac{d^3 y}{dx^3} \right|_{x=x_m} = \frac{d}{x_e^3} \left[60 - 360\left(\frac{x_m}{x_e}\right) + 360\left(\frac{x_m}{x_e}\right)^2 \right] = 0 \tag{23}$$

Solving this equation, we obtain

$$\frac{x_m}{x_e} = \frac{\left(3 - \sqrt{3}\right)}{6} = 0.2113 \tag{24}$$

κ_{max} is obtained by substituting $\dfrac{d^2 y}{dt^2}$ in the right side of equation (22) to the lateral acceleration limit, a_{max}. Then, x_e can be written as

$$x_e = V\sqrt{\dfrac{d}{a_{max}}\left\{60\dfrac{x_m}{x_e} - 180\left(\dfrac{x_m}{x_e}\right)^2 + 120\left(\dfrac{x_m}{x_e}\right)^3\right\}}.$$ (25)

Recalling $dx \approx V\,dt$, we note that $x \approx Vt$ if V does not vary much. Thus, y can be expressed as a function of time by substituting $x=Vt$ in equation (19).

$$y(t) = d\left\{10\left(\dfrac{Vt}{x_e}\right)^3 - 15\left(\dfrac{Vt}{x_e}\right)^4 + 6\left(\dfrac{Vt}{x_e}\right)^5\right\}$$ (26)

The transition time is obtained by

$$T_{pol} = \dfrac{x_e}{V}$$ (27)
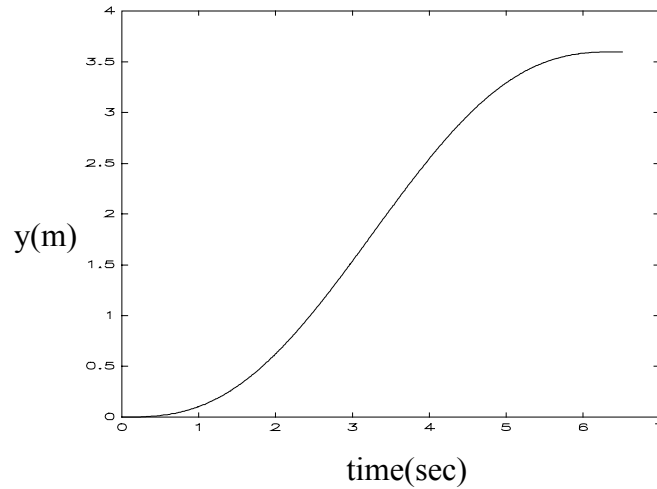
The trajectory is shown in figure 4.

Figure 4: Polynomial VDT

(4) Trapezoidal Acceleration Trajectory

While the 5th order polynomial trajectory has a continuous curvature and a simple closed-form, it is difficult to parameterize the trajectory in terms of lateral jerk and its required transition time is longer than the previous two trajectories as shown in figure 3.

To reduce the transition time and parameterize the lateral jerk more explicitly, the trapezoidal acceleration trajectory is designed. For this trajectory, the acceleration profile is specified as shown in figure 5. Here, the jerk is slope of the acceleration profile.
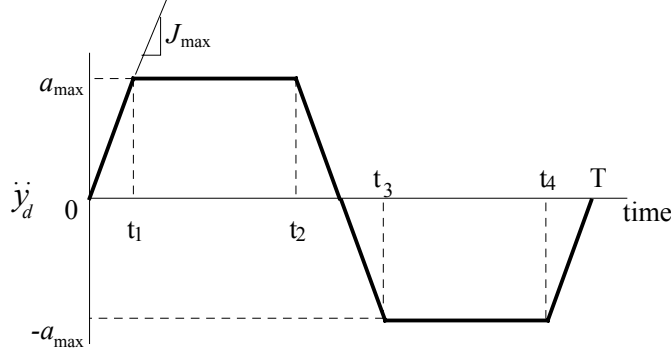

Figure 5: Trapezoidal Acceleration Profile

From this figure, the desired lateral acceleration, $\ddot{y}_d$, can be written as

$$\begin{aligned}
\ddot{y}_d &= J_{max}t \cdot u(t) - J_{max}(t - t_1) \cdot u(t - t_1) - J_{max}(t - t_2) \cdot u(t - t_2) \\
&+ J_{max}(t - t_3) \cdot u(t - t_3) + J_{max}(t - t_4) \cdot u(t - t_4) - J_{max}(t - T) \cdot u(t - T)
\end{aligned} \tag{28}$$

where, J_{max} is the jerk limit and $u(t)$ is a unit step function. Temporal parameters for this trajectory, $t_1, t_2, t_3, t_4,$ and $T,$ are given as

$$t_1 = \frac{a_{max}}{J_{max}}, \quad t_2 = \frac{-t_1^2 + \sqrt{t_1^4 + 4t_1\dfrac{d}{J_{max}}}}{2t_1} \tag{29}$$

$$t_3 = 2t_1 + t_2, \quad t_4 = t_1 + 2t_2, \quad T = 2t_1 + 2t_2$$

As shown in equation (29), the parameters, $t_1, t_2, t_3,$ and t_4 as well as T depends on $\dfrac{a_{max}}{J_{max}}$ and the constraining equation , $y(T) = d.$ Several trajectories with different values of the jerk limit for the same lateral acceleration limit, 0.05g/sec, are shown in figure 6. Here, $J_{max} = 0.7829 \ m/s^3$ corresponds to the initial jerk of the polynomial trajectory. As shown in figure 6, the time for lane change gets shorter as the limit becomes larger. In

the limiting case when the jerk is infinity, the acceleration makes step changes and trapezoidal acceleration trajectory is reduced to the circular trajectory.
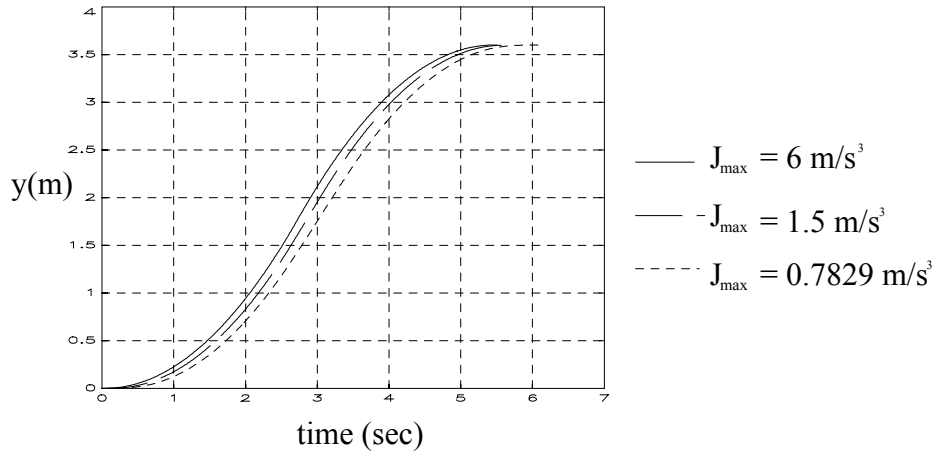

Figure 6: Trapezoidal Acceleration Trajectories

Since t_1 is a function of jerk, t_2 can also be expressed as a function of jerk as

$$t_2 = -\frac{1}{2}\frac{a_{max}}{J_{max}} + \frac{1}{2}\sqrt{\left(\frac{a_{max}}{J_{max}}\right)^2 + 4\frac{d}{a_{max}}} . \qquad (30)$$

Then, the transition time, T, can be written as

$$T = 2(t_1 + t_2) = \frac{a_{max}}{J_{max}} + \sqrt{\left(\frac{a_{max}}{J_{max}}\right)^2 + 4\frac{d}{a_{max}}} . \qquad (31)$$

The relation between the jerk limit, J_{max}, and the total transition time, T, with a fixed maximum acceleration is shown in figure 7. Note that the transition time is asymptotic to that for the circular trajectory, shown by the dotted line, as the jerk limit is increased to infinity.

Figure 8 shows relation between the transition time and the lane width. In this plot, the lateral acceleration limit and the lateral jerk limit are selected as 0.05g and 0.1g/s, respectively. As shown in figure 8, the transition time increases as the lane width increases, which can be confirmed from equation (31). Here, 3.6 meter corresponds to the current highway lane width and 3.0 meter corresponds to the body width of a large car such as Lincoln Town Car, which is the possible lower limit for the lane width.
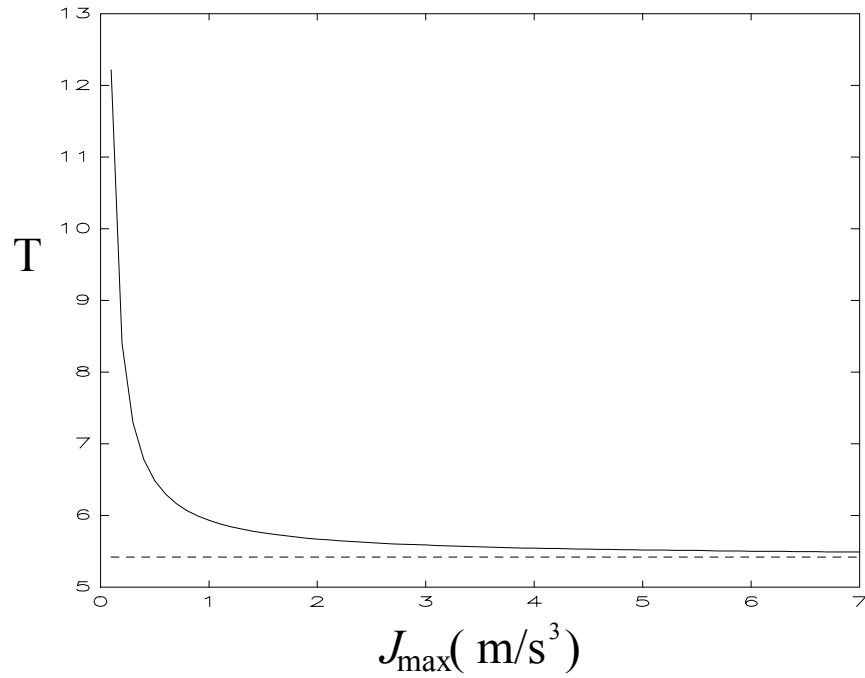
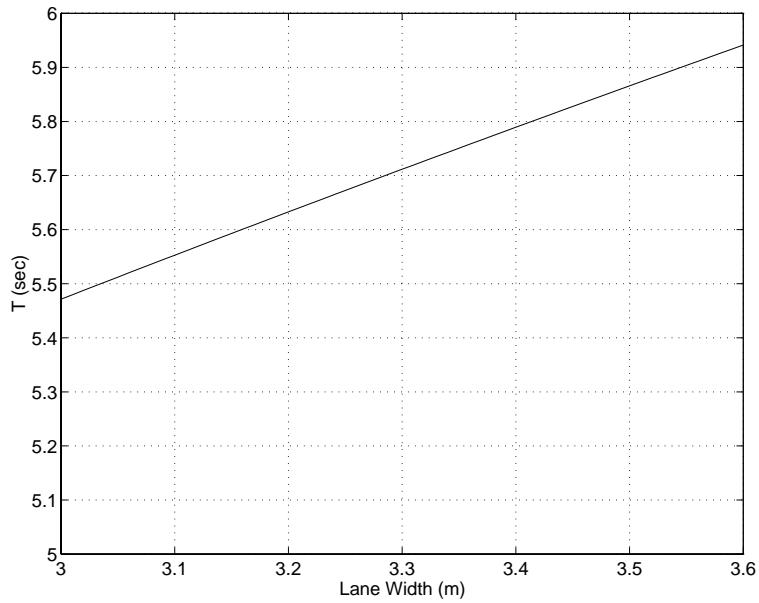Figure 7: Relation between Jerk Limit and T

Figure 8: Relation between Lane Width and T

The transition time for different trajectories, discussed above, are shown in figure 9 for V= 31.1m/sec (70 MPH), a_{max}= 0.05g, and J_{max}= 0.1 g/s.

Transition time (sec)

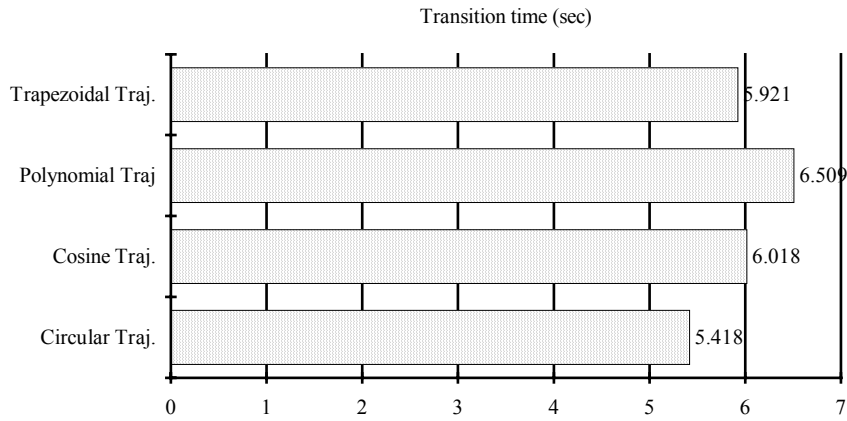|		
Trapezoidal Traj.		5.921
Polynomial Traj		6.509
Cosine Traj.		6.018
Circular Traj.		5.418

0   1   2   3   4   5   6   7

Figure 9. Comparison of Transition Times

Considering this comparison of the transition time and the specification of the ride comfort constraints, the trapezoidal acceleration trajectory may be the most desirable candidate for the VDT of a lane change maneuver. In the rest of this report, the trapezoidal acceleration trajectory is selected as the VDT.

4. Uncertainty Analysis

The vehicle model given by equations (1) and (2) includes parameters such as m and C_s as well as external disturbances such as wind drag. Three parameters, which affect the vehicle dynamics significantly, are the cornering stiffness, mass and moment of inertia about the vertical axis (Peng and Tomizuka 1991). The possible range for each of these three parameters is given in table 2.

Cornering Stiffness (C_s)	$0.2 \sim 2.0\ C_{s\ nominal}$
Mass (m)	$0.85 \sim 1.15\ m_{nominal}$
Moment of Inertia about Vertical Axis (I_z)	$0.85 \sim 1.15\ I_{z\ nominal}$

Table 2. Range of Parameters

The performance of the control system must be robust under the variation of these parameters. In this chapter, it will be shown that the performance of a lane change maneuver is significantly affected by the variation of these parameters under open loop control. Furthermore, an analysis will be performed to determine how these parameters affect the system parameters A_is and B_is. This result will be utilized later in the design of a nonlinear robust controller.

To observe the effects of parameter variations and disturbances on the vehicle response, open loop simulations were performed, and representative results are shown in figure 10. In this simulation, the control input is calculated using the transfer function of the nominal linear model from steering angle to $\ddot{y}$, the lateral acceleration that is obtained by differentiating y twice (see Appendix 1). By inverting this transfer function, we obtain the transfer function from $\ddot{y}$ to steering angle. After substituting the Laplace transform of $\ddot{y}_d$ for $\ddot{y}$, one obtain the open loop control input under nominal conditions. The detailed derivation is in appendix 1. As an example, the steering input corresponding to a VDT with the trajectory parameters given in table 1 (page 4) is shown in figure 11.

Since the variations of mass and moment of inertia are smaller than that of cornering stiffness, they affect the lane change maneuver less seriously than cornering stiffness change and wind disturbance. Thus, only the effects of the variation of the cornering stiffness and the wind disturbances are shown in figure 10.

Treating all the uncertainties in the system parameters as being additive, we can define the uncertainty of each parameter as follows.

$$A_1 = \hat{A}_1\left(1+\Delta A_1\right) \ , \ \ A_2 = \hat{A}_2\left(1+\Delta A_2\right) \ , \ \ A_3 = \hat{A}_3\left(1+\Delta A_3\right) \ , \ \ A_4 = \hat{A}_4\left(1+\Delta A_4\right)$$
$$B_1 = \hat{B}_1\left(1+\Delta B_1\right) \ , \ \ B_2 = \hat{B}_2\left(1+\Delta B_2\right)$$

(32)

With some manipulation of equation (32), we can find that these uncertainty terms are bounded by a constant, and written as

$$\left|\Delta A_i\right| \leq \alpha \quad , \quad 1 \leq i \leq 4$$
$$\left|\Delta B_j\right| \leq \beta \quad , \quad 1 \leq j \leq 2.$$
$$\alpha = \beta = 1.3529$$

(33)

These uncertainty bounds will be used in chapter 6 for the design of the nonlinear controller. The detailed derivation of equation (33) can be found in appendix 2.
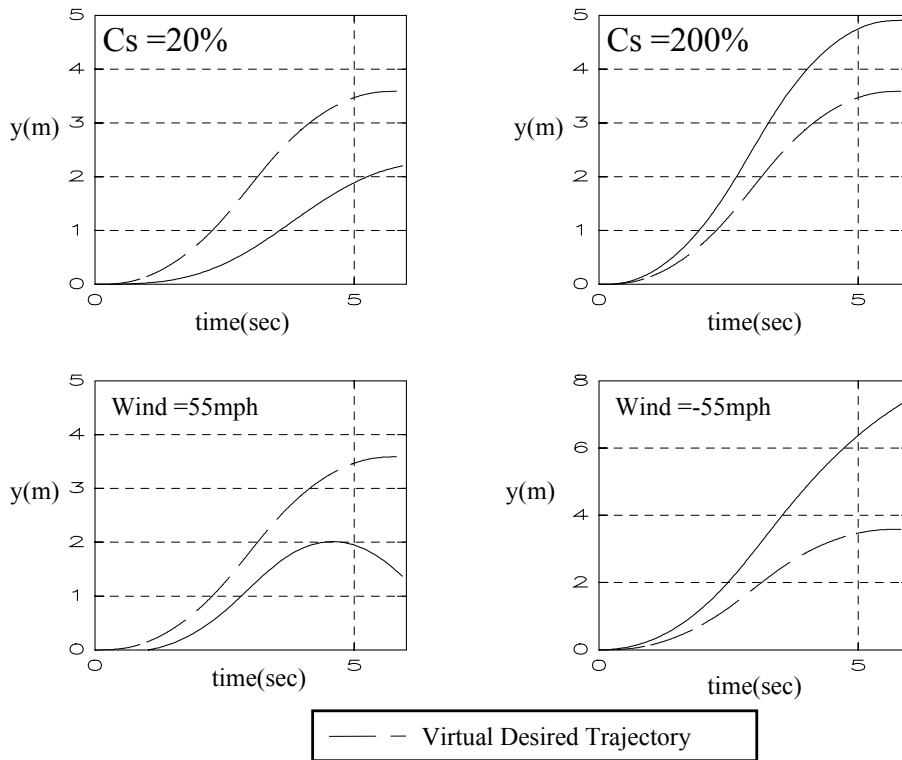

Figure 10: Uncertainty Analysis
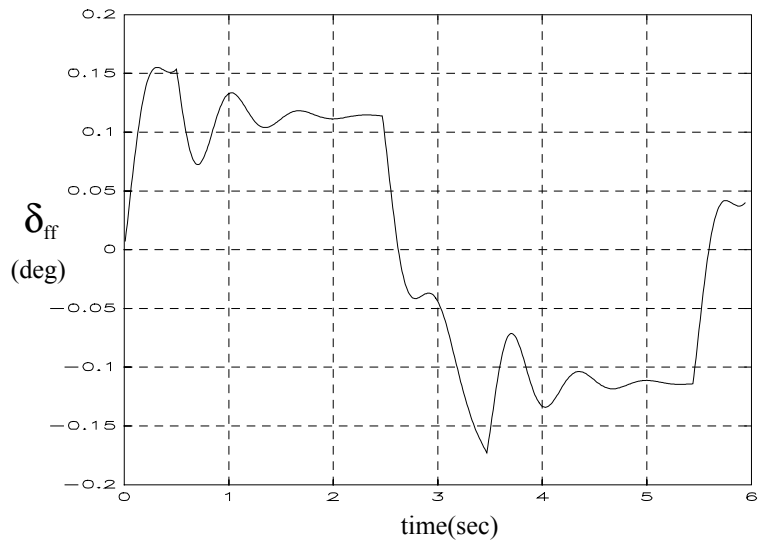(% means the ratio to nominal value)

Figure 11: Control Input For Open Loop Simulation

5. LQ / FSLQ Controller

As shown in figure 11, the lane change maneuver cannot be performed in an open loop manner. In this chapter, two optimal controllers are designed to overcome the effects of the uncertainties. They are linear quadratic (LQ) optimal controller and frequency shaped linear quadratic (FSLQ) optimal controller. These two controllers use the linear vehicle model, which omit the nonlinear term in equation (1). Thus, wind force term in equation (1) is not included in the linear model. The controllers are designed for the nominal values of the system parameters.

Defining the states of the system as

$$\mathbf{x} = \begin{bmatrix} x_1 & x_2 & x_3 & x_4 \end{bmatrix}^T = \begin{bmatrix} y & \dot{y} & \varepsilon & \dot{\varepsilon} \end{bmatrix}^T, \tag{34}$$

the linear model can be written in the state space description.

$$\frac{d}{dt} \begin{bmatrix} x_1 \\ x_2 \\ x_3 \\ x_4 \end{bmatrix} = \underbrace{\begin{bmatrix} 0 & 1 & 0 & 0 \\ 0 & \dfrac{A_1}{V} & -A_1 & \dfrac{A_2}{V} \\ 0 & 0 & 0 & 1 \\ 0 & \dfrac{A_3}{V} & -A_3 & \dfrac{A_4}{V} \end{bmatrix}}_{\mathbf{A}} \begin{bmatrix} x_1 \\ x_2 \\ x_3 \\ x_4 \end{bmatrix} + \underbrace{\begin{bmatrix} 0 \\ B_1 \\ 0 \\ B_2 \end{bmatrix}}_{\mathbf{B}} \delta$$

$$\text{or} \tag{35}$$

$$\dot{\mathbf{x}} = \mathbf{A}\mathbf{x} + \mathbf{B}\delta$$

If we decompose δ into a feedforward part and a feedback part, and define $\mathbf{x}_d$ as a response to the feed forward input, equation (35) can be written as

$$\delta\dot{\mathbf{x}} = \mathbf{A}\delta\mathbf{x} + \mathbf{B}\delta_{fb} \tag{36}$$

where

$$\begin{aligned} \delta\mathbf{x} &= \mathbf{x} - \mathbf{x_d} \\ \delta_{fb} &= \delta - \delta_{ff} \end{aligned} \tag{37}$$

Here, the feedforward control input, δ_{ff}, is taken as the control input for the open loop simulation. Since this control input makes the vehicle follow the VDT under nominal conditions, it can be used as a feedforward input for this tracking problem. This change

of variables converts the tracking problem into a regulation problem, which is the standard form for applying LQ or FSLQ controller design techniques.

The LQ controller is designed for the feed back control input, δ_{fb}, with the following infinite horizon cost function.

$$J = \int_0^\infty \left\{ \delta\mathbf{x}^T \mathbf{Q} \delta\mathbf{x} + r\delta_{fb}^2 \right\} dt \tag{38}$$

where

$$\mathbf{Q} = \begin{bmatrix} 1 & 0 & 0 & 0 \\ 0 & 1 & 0 & 0 \\ 0 & 0 & 1 & 0 \\ 0 & 0 & 0 & 1 \end{bmatrix}, \ r = \text{constant}. \tag{39}$$

While the tracking error converges to zero with this controller, the input generated by this algorithm may make the response of the vehicle violate the ride comfort constraint. To prevent this, the FSLQ controller is designed for the lane change maneuver.

Peng and Tomizuka (1991) designed the FSLQ controller for lane following control and their experimental results confirmed the effectiveness of this controller. Cost function of the FSLQ controller is written as

$$J = \frac{1}{2} \int_0^\infty \left\{ \mathbf{z}^T \mathbf{Q} \mathbf{z} + r\delta_{fb}^2 \right\} dt \tag{40}$$

where

$$\mathbf{z} = \begin{bmatrix} z_1 & z_2 & z_3 & z_4 \end{bmatrix}^T \tag{41}$$

and

$$\dot{z}_1(t) = -\frac{1}{\lambda_a} z_1(t) + \frac{q_a}{\lambda_a} \left[\begin{bmatrix} 0 & \dfrac{A_1}{V} & -A_1 & \dfrac{A_2}{V} \end{bmatrix} \cdot \mathbf{x} + B_1 \delta \right]$$

$$\dot{z}_2(t) = -\frac{1}{\lambda_y} z_2(t) + \frac{q_y}{\lambda_y} y_r(t)$$

$$\dot{z}_3(t) = -\frac{1}{\lambda_\varepsilon} z_3(t) + \frac{q_\varepsilon}{\lambda_\varepsilon} \left(\varepsilon(t) - \varepsilon_d(t) \right) \tag{42}$$

$$\dot{z}_4(t) = q_i \begin{bmatrix} 1 & 0 & d_s & 0 \end{bmatrix} \cdot \mathbf{x}$$

Here, q_a, q_y, q_ε and q_i are the gains of the frequency dependent weightings, and λ_a, λ_y, and λ_ε are the corresponding cut off frequencies. $\mathbf{Q}$ and r are defined as (39).

This cost function is different from equation (38) in penalizing the feedback term more in the low frequency region (i.e. The cost function is chosen with filtered signals of

- 20 -

system states). This frequency shaping has been adopted for achieving ride comfort and robustness to high frequency disturbances. Thus, the control input generated by this controller shows smoother lateral response than the LQ optimal controller. For the lane change maneuver, the lane following FSLQ controller is modified so that it uses the tracking error, equation (37). As explained earlier, one of the significant difference between the lane following and the lane change maneuvers is the method of obtaining the lateral position of the vehicle. While the lateral position for the lane following controller can be measured directly, the lateral position for the lane change controller is obtained indirectly by integrating the lateral accelerometer twice.

6. Sliding Mode Controller

Since the lateral wind force is modeled as a nonlinear term in equation (1), a nonlinear controller is also considered. To obtain such a controller, a sliding mode controller is designed using the nonlinear simplified model.

The tracking error is defined as

$$e(t) = \{y(t) - y_d(t)\} + \psi \{\varepsilon(t) - \varepsilon_d(t)\} \tag{1}$$

where, y_d and ε_d are the desired lateral position and the desired yaw angle of the vehicle, which are obtained from the VDT. Here, ψ is a dimension conversion factor and a weighting factor at the same time. In the following, ψ is assumed to be 1 for the convenience of the calculation.

The sliding mode controller attempts to make the tracking error signal given by equation (43) converge to zero in the presence of the system parameter variations and disturbances. Normally, sliding mode control makes the control input sensitive to small errors: i.e. high gain control results. High gain control for δ implies that δ must change rapidly, which is not practical and may degrade ride comfort. To overcome this problem, we propose to filter the tracking error by

$$v(t) = \int_0^t \gamma^{t-\tau} e(\tau) d\tau, \; 0 < \gamma < 1 \tag{2}$$

v(t) can be regarded as the output of the filter

$$\frac{dv(t)}{dt} - (\ln \gamma) \cdot v(t) = e(t). \tag{3}$$

Considering the transfer function of the linear model, equation (A.1.1), the vehicle system has a relative degree of 2, which means that the degree of the denominator of the transfer function is larger than that of the numerator by two. Therefore, we define a second order sliding surface in terms of *v(t)*: i.e.

$$S(t) = \left(\frac{d}{dt} + \lambda\right)^2 v(t) = \left(\frac{d}{dt} + \lambda\right)^2 \int_0^t \gamma^{(t-\tau)} e(\tau) d\tau = 0 \tag{4}$$

Notice that *v(t)* converges to zero when the system states are on the sliding surface. From equation (46), we obtain

$$\dot{S} = \dddot{v} + 2\lambda\ddot{v} + \lambda^2\dot{v} \tag{5}$$

Derivatives of *v(t)* are obtained as

$$\dot{v}(t) = \frac{d}{dt}\int_0^t \gamma^{t-\tau}e(\tau)d\tau \tag{6}$$
$$= (\ln\gamma)\cdot v(t) + e(t)$$

$$\ddot{v}(t) = \frac{d}{dt}\dot{v}(t) \tag{7}$$
$$= (\ln\gamma)^2 v(t) + (\ln\gamma)\cdot e(t) + \dot{e}(t)$$

$$\dddot{v}(t) = \frac{d}{dt}\ddot{v}(t) \tag{8}$$
$$= (\ln\gamma)^3 v(t) + (\ln\gamma)^2 e(t) + (\ln\gamma)\cdot\dot{e}(t) + \ddot{e}(t)$$

From equations (48), (49) and (50), $S(t)$ and $\dot{S}(t)$ can be written as

$$S = (\lambda + \ln\gamma)^2 v + (2\lambda + \ln\gamma)e + \dot{e} \tag{9}$$

$$\dot{S} = \ln\gamma\cdot(\lambda + \ln\gamma)^2 v + (\lambda + \ln\gamma)^2 e + (2\lambda + \ln\gamma)\dot{e} + \ddot{e}. \tag{10}$$

Substituting equation (43) into equation (52), we obtain

$$\dot{S} = \ln\gamma\cdot(\lambda + \ln\gamma)^2 v + (\lambda + \ln\gamma)^2 e + (2\lambda + \ln\gamma)\dot{e} + \ddot{e}$$
$$= \left(\frac{A_1 + A_3}{V}\right)\dot{y} - (A_1 + A_3)\varepsilon + \left(\frac{A_2 + A_4}{V}\right)\dot{\varepsilon} - \frac{K_y}{m}\left(V_{wy} + \dot{y} - V\varepsilon\right)\left|V_{wy} + \dot{y} - V\varepsilon\right| \tag{11}$$
$$+ (B_1 + B_2)\delta - \ddot{y}_d - \ddot{\varepsilon}_d + (2\lambda + \ln\gamma)\dot{e} + (\lambda + \ln\gamma)^2 e + \ln\gamma\cdot(\lambda + \ln\gamma)^2 v$$

Now, substitute the nominal conditions, i.e. the nominal parameter values and $V_{wy} = 0$, in the right hand side of equation (53) and equate it to $-K\cdot sgn(S)$: i.e.

$$\left(\frac{\hat{A}_1 + \hat{A}_3}{V}\right)\dot{y} - \left(\hat{A}_1 + \hat{A}_3\right)\varepsilon + \left(\frac{\hat{A}_2 + \hat{A}_4}{V}\right)\dot{\varepsilon} - \frac{K_y}{m}(\dot{y} - V\varepsilon)|\dot{y} - V\varepsilon|$$

$$+ \left(\hat{B}_1 + \hat{B}_2\right)\delta - \ddot{y}_d - \ddot{\varepsilon}_d + (2\lambda + \ln\gamma)\dot{e}(t) + (\lambda + \ln\gamma)^2 e(t) + \ln\gamma \cdot (\lambda + \ln\gamma)^2 v(t) \quad (12)$$

$$= -K \cdot \text{sgn}(S)$$

where K is called the robustness term, which will cancel all the uncertain dynamics in the control system. This term will be determined later.

From equation (54), the control input δ is determined as

$$\delta = \frac{1}{\hat{B}_1 + \hat{B}_2}\left\{\begin{array}{l} -\dfrac{\left(\hat{A}_1 + \hat{A}_3\right)}{V}\dot{y} + \left(\hat{A}_1 + \hat{A}_3\right)\varepsilon - \dfrac{\left(\hat{A}_2 + \hat{A}_4\right)}{V}\dot{\varepsilon} + \dfrac{K_y}{\hat{m}}(\dot{y} - V\varepsilon)|\dot{y} - V\varepsilon| + \ddot{y}_d + \ddot{\varepsilon}_d \\ -(2\lambda + \ln\gamma)\dot{e} - (\lambda + \ln\gamma)^2 e - \ln\gamma \cdot (\lambda + \ln\gamma)^2 v - K \cdot \text{sgn}(S) \end{array}\right\} (13)$$

The sliding surface S = 0 is attractive, which assures the stability of the system, if the right hand side of equation (53) is bounded by $-\eta \cdot sgn(S)$ with the control input δ of equation (55): i.e. for stability, we need

$$\dot{S} = \frac{\left(\hat{A}_1\Delta A_1 + \hat{A}_3\Delta A_3\right)}{V}\dot{y} - \left(\hat{A}_1\Delta A_1 + \hat{A}_3\Delta A_3\right)\varepsilon + \frac{\left(\hat{A}_2\Delta A_2 + \hat{A}_4\Delta A_4\right)}{V}\dot{\varepsilon}$$

$$- \frac{K_y}{m}\left[(V_{wy} + \dot{y} - V\varepsilon)|V_{wy} + \dot{y} - V\varepsilon| - (\dot{y} - V\varepsilon)|\dot{y} - V\varepsilon|\right] - K \cdot \text{sgn}(S)$$

$$+ \frac{\left(\hat{B}_1\Delta B_1 + \hat{B}_2\Delta B_2\right)}{\left(\hat{B}_1 + \hat{B}_2\right)}\left\{\begin{array}{l} -\dfrac{\left(\hat{A}_1 + \hat{A}_3\right)}{V}\dot{y} + \left(\hat{A}_1 + \hat{A}_3\right)\varepsilon - \dfrac{\left(\hat{A}_2 + \hat{A}_4\right)}{V}\dot{\varepsilon} + \dfrac{K_y}{\hat{m}}(\dot{y} - V\varepsilon)|\dot{y} - V\varepsilon| \\ +\ddot{y}_d + \ddot{\varepsilon}_d - (2\lambda + \ln\gamma)\dot{e} - (\lambda + \ln\gamma)^2 e - \ln\gamma \cdot (\lambda + \ln\gamma)^2 v \\ -K \cdot \text{sgn}(S) \end{array}\right\} (14)$$

$$\leq -\eta \cdot \text{sgn}(S)$$

In this inequality, as η becomes larger, S converges to zero faster. Thus, we can adjust the controller performance by choosing η appropriately.

To check the validity of the inequality, we first note

$$(V_{wy} + \dot{y} - V\varepsilon)\left|V_{wy} + \dot{y} - V\varepsilon\right| - (\dot{y} - V\varepsilon)\left|\dot{y} - V\varepsilon\right|$$

$$\leq (V_{wy} + \dot{y} - V\varepsilon)\left\{\left|V_{wy}\right| + \left|\dot{y} - V\varepsilon\right|\right\} - (\dot{y} - V\varepsilon)\left|\dot{y} - V\varepsilon\right|$$

$$\leq V_{wy}\left|V_{wy}\right| + 2\left|V_{wy}\right| \cdot \left|\dot{y} - V\varepsilon\right| \tag{15}$$

$$\leq V_{wm}^{\;2} + 2V_{wm} \cdot \left|\dot{y} - V\varepsilon\right| \quad , \quad V_{wm} = \max\left(\left|V_{wy}\right|\right)$$

Inequality (57) corresponds to the bounds for the lateral wind force.

This inequality is combined with other bounds for uncertainties that are derived in appendix 2 to yield

$$K \geq \eta + 2\alpha \left|\frac{\left(\hat{A}_1 + \hat{A}_3\right)}{V}\dot{y} - \left(\hat{A}_1 + \hat{A}_3\right)\varepsilon + \frac{\left(\hat{A}_2 + \hat{A}_4\right)}{V}\dot{\varepsilon}\right|$$

$$+ \frac{K_y}{\hat{m}}\left\{V^2_{wm} + \left[2V_{wm} + \alpha\left|\dot{y} - V\varepsilon\right|\right]\left|\dot{y} - V\varepsilon\right|\right\} \tag{16}$$

$$+ \alpha\left|\ddot{y}_d + \ddot{\varepsilon}_d - (2\lambda + \ln\gamma)\dot{e} - (\lambda + \ln\gamma)^2 e - \ln\gamma(\lambda + \ln\gamma)^2 v\right|$$

The robustness term K in equation (55) must satisfy equation (58). Since the "sign" function in equation (54) causes the chattering problem when $S \approx 0$, $K \cdot S$ is used instead of $K \cdot sgn(S)$ to remove the chattering of the control for actual implementation.

Figure 12 shows the effect of the changes of γ on the controller performance when the cornering stiffness is set to 0.2 times its nominal value. Here, we can see that peak of the steering angle, δ_{actual}, is reduced as γ becomes smaller, especially during the time period, $0 \sim 1$ sec. Accordingly, the corresponding acceleration and jerk are also reduced, which in turn mean ride comfort enhancement. The sliding mode control with the filter can be said to maintain its tracking performance in terms of the final position error. In addition, the overshoot of position error is reduced.

If $\gamma = 1.0$, $v(t)$ becomes the integral of the error signal, which is used for the usual sliding mode controller. γ may be viewed as a forgetting factor for $e(t)$ because it reduces the memory of $e(t)$ in equation(44).
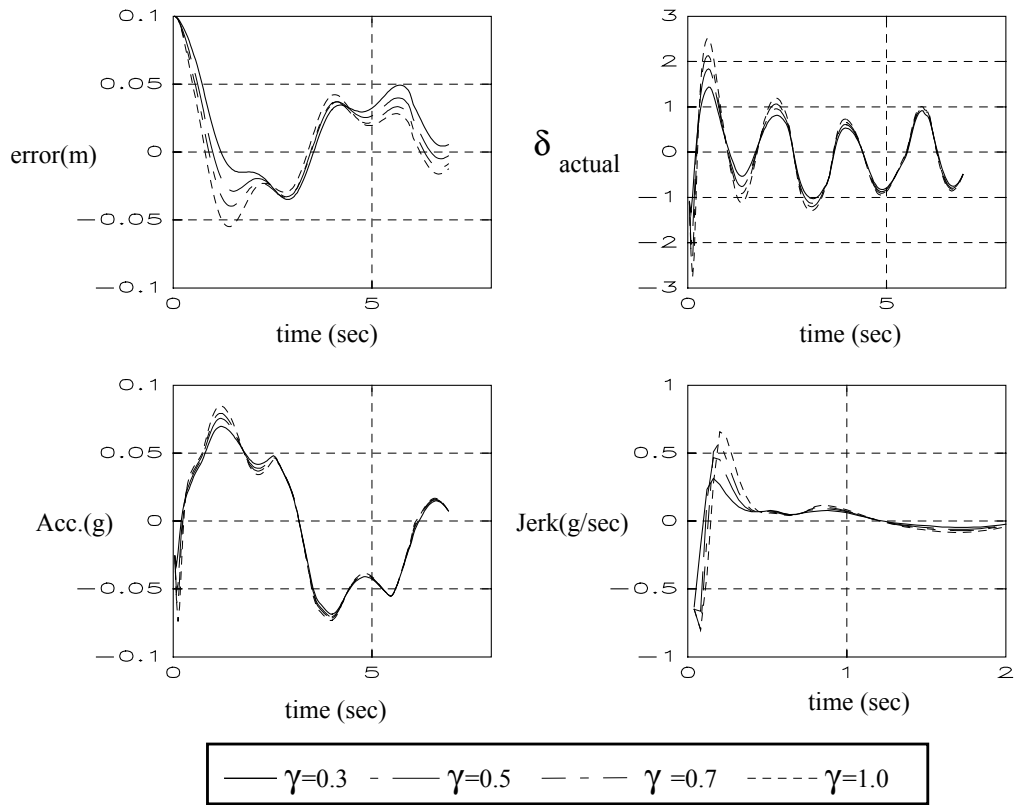
Figure 1: Effect of γ.

7. Simulation Results

In the simulation of the controllers designed in the previous chapters, the vehicle speed is set to 31.1m/sec (70 MPH), the lateral acceleration limit for the VDT is set to 0.05g, and the jerk limit is set to 0.1g/sec. With these values, total transition time is obtained as 5.92 seconds (refer to figure 9).

The control gains for the LQ controller are obtained by using MATLAB. The gain vector, $\mathbf{k}$, used in the simulation is

$$\mathbf{k} = \begin{bmatrix} 7.6274269e\text{-}03 \\ 4.8276297e\text{-}03 \\ 2.4164644e\text{-}01 \\ 4.5495866e\text{-}02 \end{bmatrix} \tag{17}$$

For the sliding mode controller, the following values are chosen after testing the controller with various controller parameters.

λ	5
η	50
Error! Not a valid embedded object.	0.3

Table 3. Parameters for Sliding Mode Controller

7.1 Comparison of Robustness to System Parameter Uncertainty

As mentioned earlier, the variations in the mass and the moment of inertia have a smaller effect on the lane change maneuver than variations in cornering stiffness and wind disturbance. In this report, changes in cornering stiffness and wind gust are considered in order to evaluate the performance of the controllers.

In figure 13, cornering stiffness is set to 0.2 times its nominal value. This cornering stiffness value corresponds to an extremely slippery road condition. As shown in figure 13, the position error with respect to the VDT under the sliding mode control is smaller than that under the LQ or the FSLQ control. However, the sliding mode controller produces larger steering commands than the LQ and the FSLQ controllers

during most of the maneuver period. The maneuver under the FSLQ control shows larger variation in the lateral acceleration and the position error than other controllers. Thus, it can be concluded that the FSLQ controller is less robust to the varying cornering stiffness than the LQ and the sliding mode controllers.

In figure 14, the effect of wind disturbance is studied. The position errors near the end of the maneuver are nearly the same for the maneuvers under the sliding mode control and the FSLQ control while the error for the LQ control is larger than for the two controllers. Even if the position errors under the two control converges to the same value at the end of the maneuver, the position error variation under the sliding mode control is different from the one under the FSLQ control in that the former converges without overshooting, while the latter converges with overshooting. In this simulation, the lateral acceleration under the FSLQ control shows larger variation. From this figure, it can be concluded that the LQ controller is less robust to the lateral wind disturbances than the FSLQ and the sliding mode controllers.
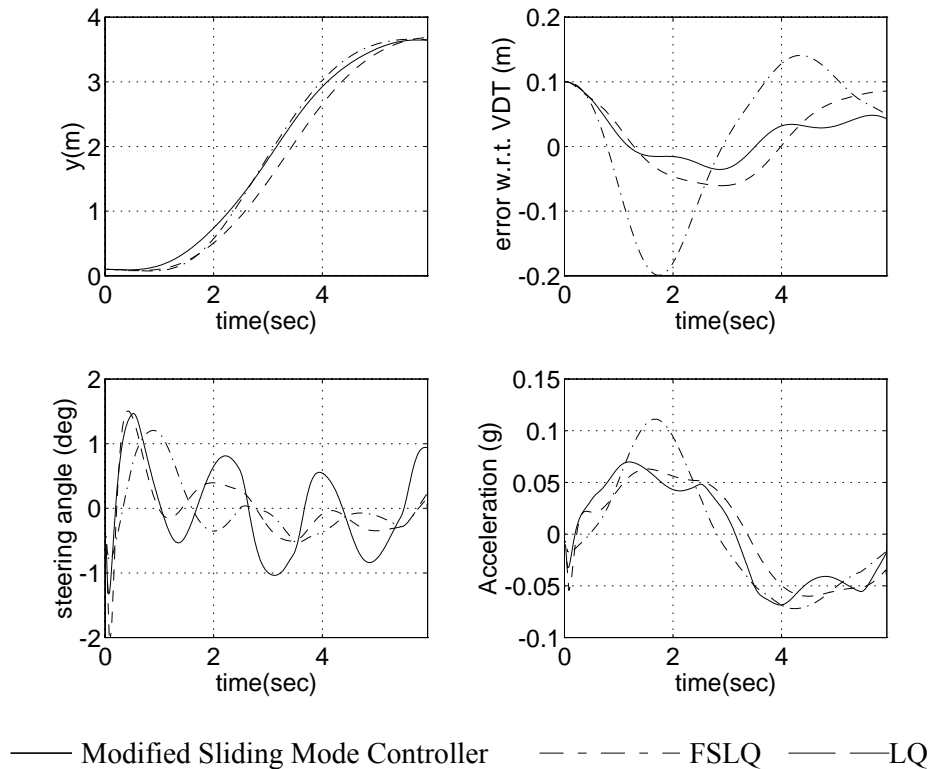

———— Modified Sliding Mode Controller   – – – – – FSLQ   —— ——LQ

Figure 2. Comparison of Controllers Using Onboard Sensors
(Cs = 20% nominal, Initial Error : 0.1m, 0.1^{o})

7.2 Robustness to Combined Uncertainties

So far, the effects of individual uncertainties have been studied. To evaluate the controller performance with combined uncertainties, the following scenario is used for simulation.

Variations of cornering stiffness : 0~1 sec - nominal value

1~3 sec - 20% of nominal value

3~4 sec - nominal value

4~5 sec - 200% of nominal value

5~ sec - nominal value

24.4m/sec (55 MPH) wind gust has been blowing from 1.5 sec to 5 sec.
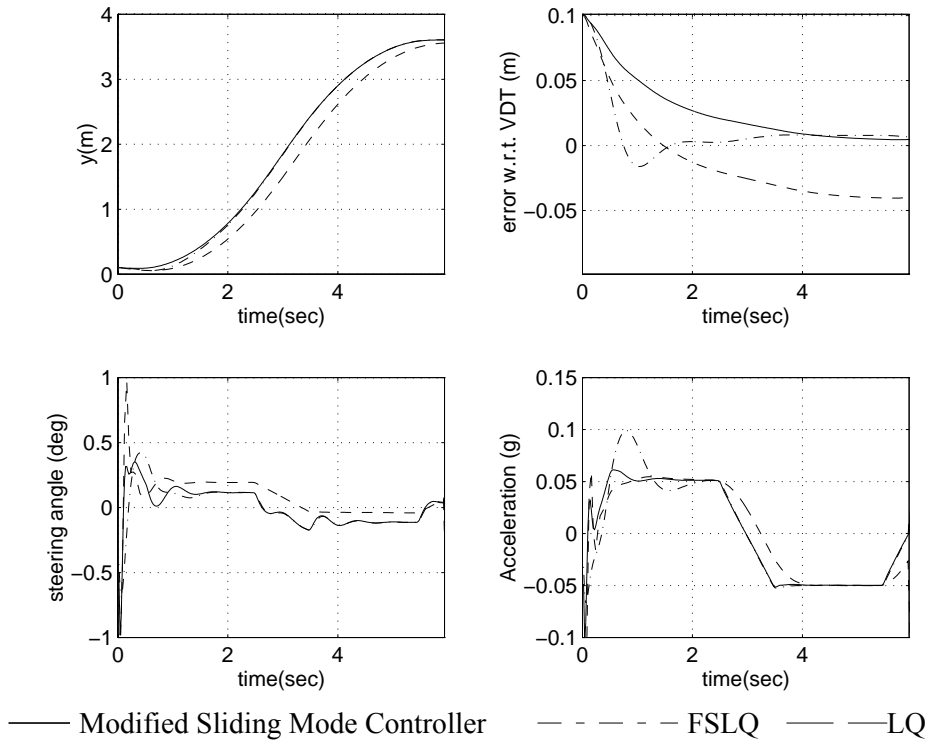

—— Modified Sliding Mode Controller   — - — - — FSLQ   —— ——LQ

Figure 3. Comparison of Controllers Using On-Board Sensors
(Wind = 24.4m/sec, Initial Error : 0.1m, 0.1$^{\text{o}}$)

As shown in figure 15, only the sliding mode controller can finish the maneuver without the final position error. In addition, the variations in the position error and the lateral acceleration under this control algorithm are less than under the LQ control or the FSLQ control. The FSLQ controller can achieve the maneuver with less control action while maintaining moderate position error and the lateral accelerations. The LQ controlled maneuver shows large variations in the tracking error, the steering input, and lateral acceleration. From this simulation, the LQ control algorithm does not seem to be adequate for the lane change maneuver.
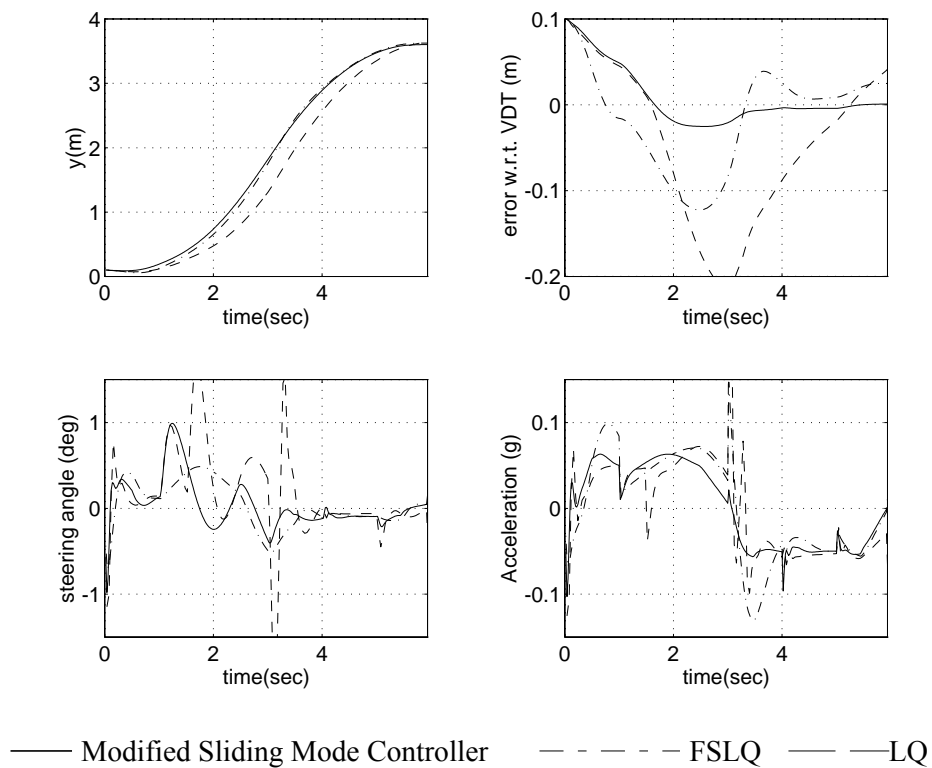

Figure 4. Comparison of Controllers Using Onboard Sensors For Scenario

From these three simulations, it can be confirmed that the sliding mode controller with a filtered error can perform lane change maneuvers with less tracking error and lateral acceleration variation compared with the LQ controller and the FSLQ controller. The FSLQ controller also can achieve the maneuvers with less control effort allowing a little larger variations in the tracking error and lateral acceleration than the sliding mode controller. Even if the LQ controller shows its robustness to the individual system uncertainties, it is vulnerable to the combined system uncertainties and disturbances.

8. Conclusion

The lane change maneuver is performed using a virtual trajectory, which is not directly measured. Among four candidates, the trapezoidal acceleration trajectory is selected as the VDT. The nominal steering input to let a vehicle follow the VDT is synthesized based on the linear model. Simulations have shown that the nominal steering input alone cannot accomplish successful lane change maneuvers because of parameter uncertainties and disturbances. The LQ controller, FSLQ controller, and the sliding mode controller have been designed to apply the closed loop tracking control of the VDT using the signals available from onboard sensors.

Simulation results show that this sliding mode controller is superior to other controllers in repelling the system uncertainties such as cornering stiffness variation and overcoming wind disturbances. For the simulation results under the stated scenarios, it can be concluded that both the sliding mode controller with a filtered error and the FSLQ controller will achieve good tracking performance under the severe hypothetical scenarios. The LQ controller shows poorer performance than the other two controllers. It may not be a candidate for further research.

9. References

[1] Caywood, W. C. et al. 1977. *Guideline for Ride-Quality Specifications Based on Transpo '72 test data*; Johns Hopkins University Applied Physics Laboratory, Washington: Urban Mass Transportation Administration, Office of Research and Development; Springfield, Va.

[2] Godthelp, J. et al. 1983. *Open and Closed Loop Steering in a Lane Change Maneuver,* Institute for Perception: National Defense Research Organization TNO group.

[3] Hess, R.A.; and A. Modjtahedzadeh. 1989. *A Preview Control Model of Driver Steering Behavior,* 1989 IEEE International Conference on Systems, Man and Cybernetics.

[4] Nelson, W. 1989. *Continuous-Curvature Path for Autonomous Vehicles,* 1989 IEEE International Conference on Robotics and Automation, pp. 1260-4.

[5] Kanayama, Y.; and B. I. Hartman. 1989. *Smooth local path planning for autonomous vehicles.,* 1989 IEEE International Conference on Robotics and Automation, pp.1265-70.

[6] Peng, H., and M. Tomizuka. 1990. *Lateral Control of Front-Wheel-Steering Rubber-Tire Vehicles,* PATH Research Report. UCB-ITS-PRR-90-5.

[7] Peng, H., and M. Tomizuka. 1991. *Optimal Preview Control For Vehicle Lateral Guidance,* PATH Research Report, UCB-ITS-PRR-91-16.

[8] Hessburg, T. et al. 1991. *An Experimental Study on Lateral Control of a Vehicle,* PATH Research Report, UCB-ITS-PRR-91-17.

[9] Hessburg, T., and M. Tomizuka. 1994. *Experimental Results of Fuzzy Logic Controller for Lateral Vehicle Guidance,* PATH Research Report, UCB-ITS-PRR-94-03.

[10] Peng, H. 1992. *Doctoral Dissertation*, University of California, Berkeley.

[11] Slotine, J.E., and W. Li. 1991. *Applied Nonlinear Control*, Prentice-Hall.

Appendix 1.
Open Loop Control Input for Nominal Linear System

The transfer function of the linear model from steering angle δ to the lateral displacement y is (Peng and Tomizuka 1990).

$$Y(s) = \frac{B_1 s^2 + \frac{B_2 A_2 - B_1 A_4}{V} s + B_1 A_3 - B_2 A_1}{s^2 \left[s^2 - \frac{A_1 + A_4}{V} s + \frac{A_1 A_4 - A_2 A_3}{V^2} + A_3 \right]} \Delta(s) \qquad \text{(A.1.1)}$$

where Y(s) is the Laplace transform of $y(t)$, and $\Delta(s)$ is the Laplace transform of $\delta(t)$.

Since $\mathsf{L}\{\ddot{y}(t)\} = s^2 \cdot Y(s)$,

$$s^2 Y(s) \equiv \mathsf{L}\{\ddot{y}(t)\}$$

$$= \frac{B_1 s^2 + \frac{B_2 A_2 - B_1 A_4}{V} s + B_1 A_3 - B_2 A_1}{\underbrace{s^2 - \frac{A_1 + A_4}{V} s + \frac{A_1 A_4 - A_2 A_3}{V^2} + A_3}_{G(s)}} \Delta(s) \qquad \text{(A.1.2)}$$

$$= G(s) \cdot \Delta(s)$$

From equation (A.1.2), the steering input to let the vehicle follow the desired acceleration profile (28), i.e. $\mathsf{L}\{\ddot{y}_d(t)\} = \frac{J}{s^2}\left\{1 - e^{-t_1 s} - e^{-t_2 s} + e^{-t_3 s} + e^{-t_4 s} - e^{-Ts}\right\}$, is

$$\Delta(s) = G(s)^{-1} \cdot \mathsf{L}\{\ddot{y}_d(t)\}$$

$$= \frac{s^2 - \frac{A_1 + A_4}{V} s + \frac{A_1 A_4 - A_2 A_3}{V^2} + A_3}{B_1 s^2 + \frac{B_2 A_2 - B_1 A_4}{V} s + B_1 A_3 - B_2 A_1} \cdot \frac{J}{s^2}\left\{1 - e^{-t_1 s} - e^{-t_2 s} + e^{-t_3 s} + e^{-t_4 s} - e^{-Ts}\right\} \qquad \text{(A.1.3)}$$

Letting $\Delta_0(s) = G(s)^{-1} \cdot \frac{J}{s^2}$,

$$\Delta(s) = \Delta_0(s) \cdot \left\{1 - e^{-t_1 s} - e^{-t_2 s} + e^{-t_3 s} + e^{-t_4 s} - e^{-Ts}\right\}. \qquad \text{(A.1.4)}$$

Then, the steering input, $\delta(t)$, is obtained by applying the inverse Laplace transformation to $\Delta(s)$. Since $\Delta(s)$ is a sum of $\Delta_0(s)$ and its delayed terms, only the inversion of $\Delta_0(s)$ is necessary.

$$\Delta_0(s) = \frac{s^2 - \dfrac{A_1 + A_4}{V}s + \dfrac{A_1 A_4 - A_2 A_3}{V^2} + A_3}{B_1 s^2 + \dfrac{B_2 A_2 - B_1 A_4}{V}s + B_1 A_3 - B_2 A_1} \cdot \frac{J}{s^2}$$

$$= \frac{J}{B_1} \cdot \frac{s^2 - \dfrac{A_1 + A_4}{V}s + \dfrac{A_1 A_4 - A_2 A_3}{V^2} + A_3}{s^2 + \dfrac{B_2 A_2 - B_1 A_4}{B_1 V}s + \dfrac{B_1 A_3 - B_2 A_1}{B_1}} \cdot \frac{1}{s^2}$$

(A.1.5)

Define

$$\bar{a} = -\frac{A_1 + A_4}{V} \quad , \quad \bar{b} = \frac{A_1 A_4 - A_2 A_3}{V^2} + A_3$$

$$\bar{c} = \frac{B_2 A_2 - B_1 A_4}{B_1 V}, \quad \bar{d} = \frac{B_1 A_3 - B_2 A_1}{B_1}$$

(A.1.6)

Then,

$$\Delta_0(s) = \frac{J}{B_1} \cdot \frac{s^2 + \bar{a}s + \bar{b}}{s^2 + \bar{c}s + \bar{d}} \cdot \frac{1}{s^2}$$

$$= \frac{J}{B_1} \left\{ \frac{as + b}{s^2} + \frac{cs + d}{s^2 + \bar{c}s + \bar{d}} \right\}$$

(A.1.7)

where

$$a = \frac{1}{\bar{d}} \left(\bar{a} - \frac{\bar{b}\bar{c}}{\bar{d}} \right) \quad , \quad b = \frac{\bar{b}}{\bar{d}}$$

$$c = -a \qquad , \quad d = 1 - \frac{\bar{b}}{\bar{d}} - \frac{\bar{c}}{\bar{d}} \left(\bar{a} - \frac{\bar{b}\bar{c}}{\bar{d}} \right)$$

(A.1.8)

Consider

$$s^2 + \bar{c}s + \bar{d} = \left(s + \frac{\bar{c}}{2} \right)^2 + \bar{d} - \frac{\bar{c}^2}{4}$$

$$= (s - \eta)^2 + \xi^2$$

(A.1.9)

where

$$\eta = -\frac{\bar{c}}{2} \quad , \quad \xi^2 = \bar{d} - \frac{\bar{c}^2}{4}.$$

(A.1.10)

Substituting equation (A.1.9) into equation (A.1.7), we can rewrite equation (A.1.7) as

$$\frac{B_1}{J} \cdot \Delta_0(s) = \frac{a}{s} + \frac{b}{s^2} + \frac{cs}{(s-\eta)^2 + \xi^2} + \frac{d}{(s-\eta)^2 + \xi^2}.$$
(A.1.11)

From this, the inversion of $\Delta_0(s)$ becomes

$$\delta_0(t) = L^{-1}\{\Delta_0(s)\}$$

$$= \frac{J}{B_1} \cdot \left[a + bt + c \frac{\sqrt{\eta^2 + \xi^2}}{\xi} e^{\eta t} \sin\left(\xi t + \tan^{-1} \frac{\xi}{\eta} \right) + d \frac{e^{\eta t}}{\xi} \sin(\xi t) \right] \cdot u(t) \text{ (A.1.12)}$$

$$= \frac{J}{B_1} \cdot \left[a + bt + c\left\{ \frac{\xi}{\eta} \sin(\xi t) + \cos(\xi t) \right\} e^{\eta t} + d \frac{e^{\eta t}}{\xi} \sin(\xi t) \right] \cdot u(t)$$

where $u(t)$ is a unit step function.

With equation (A.1.12), $\delta(t)$ can be obtained as

$$\delta(t) = \delta_0(t) - \delta_0(t - t_1) - \delta_0(t - t_2) + \delta_0(t - t_3) + \delta_0(t - t_4) - \delta_0(t - T). \quad \text{(A.1.13)}$$

Appendix 2. Derivation of Uncertainty Bounds

Each coefficient in equation (3) can be written in terms of the uncertainties in cornering stiffness, mass, and moment of inertia. A_1 can be written as

$$A_1 = \frac{-4C_s}{m} = -4\frac{\hat{C}_s(1+\Delta C_s)}{\hat{m}(1+\Delta m)} = \hat{A}_1(1+\Delta A_1) \qquad \text{(A.2.1)}$$

$$\left. \begin{array}{l} \hat{A}_1 = \dfrac{-4\hat{C}_s}{\hat{m}} \\[2ex] 1+\Delta A_1 = \dfrac{(1+\Delta C_s)}{(1+\Delta m)} \end{array} \right\} \qquad \text{(A.2.2)}$$

where $\hat{C}_s$ and $\hat{m}$ are nominal values given in table 2.1. ΔC_s and Δm are the uncertainties in parameters. In the same way, other coefficients are written as follows.

$$\left. \begin{array}{l} \hat{A}_2 = 2(l_2-l_1)\dfrac{\hat{C}_s}{\hat{m}} \\[2ex] 1+\Delta A_2 = \dfrac{(1+\Delta C_s)}{(1+\Delta m)} \end{array} \right\} \qquad \text{(A.2.3)}$$

$$\left. \begin{array}{l} \hat{A}_3 = 2(l_2-l_1)\dfrac{\hat{C}_s}{\hat{I}_z} \\[2ex] 1+\Delta A_3 = \dfrac{(1+\Delta C_s)}{(1+\Delta I_z)} \end{array} \right\} \qquad \text{(A.2.4)}$$

$$\left. \begin{array}{l} \hat{A}_4 = -2(l_1^2+l_2^2)\dfrac{\hat{C}_s}{\hat{I}_z} \\[2ex] 1+\Delta A_4 = \dfrac{(1+\Delta C_s)}{(1+\Delta I_z)} \end{array} \right\} \qquad \text{(A.2.5)}$$

As shown above, uncertainties for A_i's, ΔA_i, are in the same form. Recalling the ranges of $\Delta C_s, \Delta m, \Delta I_z$ defined in table 4.1, we find that

$$|\Delta A_i| \le \max\left[\frac{(1+\Delta C_s)}{(1+\Delta I_z)}\right] - 1 = \max\left[\frac{(1+\Delta C_s)}{(1+\Delta m)}\right] - 1 = \alpha \qquad \text{(A.2.6)}$$

Considering the actual values of $\Delta C_s, \Delta m, \Delta I_z$, $0.1739 \le \dfrac{1+\Delta C_s}{1+\Delta m} \le 2.3529$. Therefore, we obtain $\alpha = 1.3529$.

For B_i's,

$$B_1 = \frac{2\hat{C}_s}{\hat{m}} \cdot \frac{(1 + \Delta C_s)}{(1 + \Delta m)} = \hat{B}_1(1 + \Delta B_1) \tag{A.2.7}$$

$$\left.\begin{aligned} \hat{B}_1 &= \frac{2\hat{C}_s}{\hat{m}} \\ 1 + \Delta B_1 &= \frac{(1 + \Delta C_s)}{(1 + \Delta m)} \end{aligned}\right\} \tag{A.2.8}$$

and

$$B_2 = \frac{2\hat{C}_s l_1}{\hat{m}} \cdot \frac{(1 + \Delta C_s)}{(1 + \Delta m)} = \hat{B}_2(1 + \Delta B_2) \tag{A.2.9}$$

$$\left.\begin{aligned} \hat{B}_2 &= \frac{2\hat{C}_s l_1}{\hat{m}} \\ 1 + \Delta B_2 &= \frac{(1 + \Delta C_s)}{(1 + \Delta m)} \end{aligned}\right\} \tag{A.2.10}$$

Thus, from equation (A.1.6), we obtain

$$\left| \Delta B_1 \right| \leq \alpha, \text{ and } \left| \Delta B_2 \right| \leq \alpha. \tag{A.2.11}$$

Equations (A.2.6) and (A.2.11) imply that $\left| \Delta A_i \right|$ and $\left| \Delta B_i \right|$ can be bounded by the same constant.